

Article

Exploring the Dynamics of Land Surface Temperature in Jordan's Local Climate Zones: A Comprehensive Assessment through Landsat Entire Archive and Google Earth Engine

Khaled Hazaymeh , Mohammad Zeitoun, Ali Almagbile  and Areej Al Refaee

Department of Geography, Yarmouk University, Irbid 21163, Jordan; m.zeitoun@yu.edu.jo (M.Z.); a.magbile@yu.edu.jo (A.A.); areej.r@yu.edu.jo (A.A.R.)

* Correspondence: khazaymeh@yu.edu.jo

Abstract: This study aimed to analyze the trend in land surface temperature (LST) over time using the entire archive of the available cloud-free Landsat images from 1986 to 2022 for Jordan and its nine local climate zones (LCZs). Two primary datasets were used (i) Landsat-5; -8 imagery, and (ii) map of LCZs of Jordan. All LST images were clipped, preprocessed, and checked for cloud contamination and bad pixels using the quality control bands. Then, time-series of monthly LST images were generated through compositing and mosaicking processes using cloud computing functions and Java scripts in Google Earth Engine (GEE). The Mann–Kendall (MK) test and Sen's slope estimator (SSE) were used to detect and quantify the magnitude of LST trends. Results showed a warming trend in the maximum LST values for all LCZs while there was annual fluctuation in the trend line of the minimum LST values in the nine zones. The monthly average LST values showed a consistent upward trajectory, indicating a warming condition, but with variations in the magnitude. The annual rate of change in LST for the LCZs showed that the three Saharan zones are experiencing the highest rate of increase at 0.0184 K/year for Saharan Mediterranean Warm (SMW), 0.0185 K/year for Saharan Mediterranean Cool (SMC), and 0.0169 K/year for Saharan Mediterranean very Warm (SMvW), indicating rapid warming in these regions. The three arid zones came in the middle, with values of 0.0156 K/year for Arid Mediterranean Warm (AMW), 0.0151 for Arid Mediterranean very Warm (AMvW), and 0.0139 for Arid Mediterranean Cool (AMC), suggesting a slower warming trend. The two semi-arid zones and the sub-humid zone showed lower values at 0.0138, 0.0127, and 0.0117 K/year for the Semi-arid Mediterranean Cool (SaMC), Semi-arid Mediterranean Warm (SaMW) zones, and Semi-humid Mediterranean (ShM) zones, respectively, suggesting the lowest rate of change compared to other zones. These findings would provide an overall understanding of LST change and its impact in Jordan's LCZs for sustainable development and water resources demand and management.

Keywords: local warming; Google Earth Engine (GEE); Mann–Kendall; Sen's slope; trend analysis



Citation: Hazaymeh, K.; Zeitoun, M.; Almagbile, A.; Al Refaee, A. Exploring the Dynamics of Land Surface Temperature in Jordan's Local Climate Zones: A Comprehensive Assessment through Landsat Entire Archive and Google Earth Engine. *Atmosphere* **2024**, *15*, 318. <https://doi.org/10.3390/atmos15030318>

Academic Editor: Vijay P. Singh

Received: 18 January 2024

Revised: 24 February 2024

Accepted: 28 February 2024

Published: 4 March 2024



Copyright: © 2024 by the authors. Licensee MDPI, Basel, Switzerland. This article is an open access article distributed under the terms and conditions of the Creative Commons Attribution (CC BY) license (<https://creativecommons.org/licenses/by/4.0/>).

1. Introduction

Monitoring land surface temperature (LST) has emerged as a crucial factor for understanding the dynamics of Earth's ecosystems [1]. Recently, major concerns have been raised regarding the changes in the climatic conditions including the changes in LST even at local scales. In this context, the local climate zones (LCZs) are distinct geographical regions that have unique climate characteristics—they could have a significant role in shaping the microclimatic and thermal characteristics of the environment, human health, and natural ecosystems [2]. Therefore, comprehensive and accurate spatiotemporal monitoring of LST within the LCZs is essential for assessing such effects. For example, the increase in LST would influence other environmental elements such as humidity, evaporation, plants, and hydrological regimes [3,4]. Many studies have been conducted to analyze the link between

thermal behavior and environmental characteristics such as topography, land use/land cover (LULC) in local climates [5–7].

LST monitoring using traditional methods relies mainly on on-site measurements. While these techniques can yield accurate results, they often suffer from drawbacks such as high cost, time-consuming processes, and inadequate spatial coverage [2]. However, with the power of Remote Sensing (RS) technology and advanced geospatial data analysis, the study of Earth's LST patterns has been revolutionized. In this context, the Landsat satellite system—among the other satellite systems—would be the most valuable RS resource, boasting a comprehensive archive of multispectral imagery including thermal bands spanning from 1984 at fine spatial (i.e., 30 m) and temporal (i.e., 16 day) resolutions [8]. Other satellite systems provide LST data but with lower spatial resolution such as the moderate-resolution imaging spectroradiometer (MODIS, ~1 km), Advanced Very High Radiometric Resolution (AVHRR; ~1 km), the Spinning Enhanced Visible and InfraRed Imager (SEVIRI; ~3 km), and the Geostationary Operational Environmental Satellite (GOES, ~4 km). These satellite systems are suitable for monitoring LST at global and regional scales due to their low spatial resolution [9]. LST retrieval from satellite systems provides crucial insights into climate monitoring, agricultural assessments, and LCZs classification. This process relies on applying sophisticated radiative transfer models and atmospheric correction algorithms on the thermal infrared bands captured by the sensors. These spectral bands are sensitive to the emitted radiation from Earth's surface, enabling the analysis of LST variations across landscapes [10].

Monitoring LST changes and trends can be performed using (i) simple comparisons between images taken at specific time intervals (e.g., 5 or 10 years), and (ii) time-series of images taken within a specific continuous period. The first is common as it does not require an intensive computational process. Several studies have monitored LST change and linked it to the change in LULC types by employing such simple comparisons around the world. Nega and Balew [11] provided systematic reviews of published studies that analyzed the relationship between LULC changes and LST using RS data. They reviewed the most recent 100 studies around the world over the period (January/2016 to August/2021), readers are encouraged to refer to this paper for the details. However, such simple comparison may not provide an accurate overall understanding of LST changes over time due to the possible local LULC and weather variations in the selected dates [11]. Therefore, monitoring the spatiotemporal dynamics of LST using a larger amount of LST data in the form of time-series would be more effective.

2. Related Work and Original Contribution

Several studies have used time-series of MODIS products, namely MOD11C3/MYD11C3 with 0.05° (~5.6 km) and MOD11A2 and (1 km) spatial resolutions for daytime and night-time LST trend monitoring. For example, Jaber and Abu-Allaban [12] in Jordan did not find significant linear rates of change in LST in the daytime, while they observed significant linear rates of increase in LST in night-time in approximately one-third of the country, mainly in the western parts within the period 2000–2018. They concluded that anthropogenic factors would be more important in affecting the LST in night-time than the natural factors. Luintel et al. [13] in Nibal showed an increasing pattern of the night-time LST between 2000 and 2017. Dewan et al. [14] used the 8-day MODIS LST data at a 1 km spatial resolution in Bangladesh for the period 2000–2019 and reported annual warming trends in the large-populated cities. Eleftheriou et al. [15] spatially aggregated the original 1 km (8-day) LST composite into 10 km × 10 km for computing the annual and seasonal temporal trends for each sub-area in Greece. They reported a decrease in the annual and seasonal daytime LST trends, while the night-time LST trends showed an increment between 2000 and 2017. Hassan et al. [16] documented daytime cooling in LST in Summer and early Winter in the southern and southeastern natural sub-regions in Alberta province in Canada between 2001 and 2020. They indicated that several factors have influenced the LST trends in the study area including climate, LULC, geology, and topography conditions. Yang et al. [17]

analyzed the spatiotemporal patterns of LST change in the Tibetan plateau from 2000 to 2018. They indicated that both daytime and night-time showed obvious warming trends, and that the night-time variation has larger spatial coverage. Other studies have used MODIS products for LST trend analysis at larger scales, such as Liu et al. [18] for the entire world between 2003 and 2017, Yan et al. [19] for North America between 2002 and 2018, and Shawky et al. [20] in South Asia region between 2000 and 2021. In all these studies low-spatial-resolution data were used and applied to large geographic extents using few hundreds of images (i.e., 200–300 image).

Furthermore, Landsat data were used for monitoring LST over time through time-series analysis. For example, Fu and Weng [21] used Landsat-5 LST images between 2000 and 2010 and analyzed the LST time-series patterns and the intra- and inter-annual landscape thermal patterns over Los Angeles County in the United States. Their results suggested that the developed areas exhibited relatively low seasonal amplitude and that the difference of the averaged LST trend were higher in urban areas compared to other LULC types over the decade. Sekertekin et al. [22] modeled the diurnal LST in an arid environment located in Nevada in USA using the artificial neural network and time-series analysis. They used 78 Landsat-8 satellite imageries covering the study area that were utilized between 2013 and 2019. The results showed that the LST difference was lower than 1 K during wintertime and it was 2.49 K in the summertime. Athick et al. [23] used ten Landsat images from Landsat-5, -7, and -8 from 1999 to 2018 to investigate decadal LST variations and its impact on the surrounding environment in Ethiopia. They found that the barren regions had high temperatures and areas with more vegetation had low.

In all the previous studies, the researchers downloaded tens or hundreds of images over short periods (i.e., 10–20 years) from data sources to perform their analysis on local computers. However, analyzing a larger size of data for longer periods using traditional geospatial programs and local computers would be extremely tedious as they require downloading imageries that have large sizes and require complex preprocessing, input operational parameters and steps, and high-performance computational requirements. Feasibly, with the recent development of powerful geospatial analysis cloud computing platforms such as Google Earth Engine (GEE), unprecedented opportunities are opened to investigate complex environmental phenomena [24]. GEE provides access to a vast collection of global and regional RS datasets including the full archive of Landsat missions [25]. It enables the analysis of large-scale geospatial data using Google's computing infrastructure. GEE has become an important tool for the analysis of earth systems [26] including LST modeling and monitoring [27]. This platform is particularly useful in this area, as it provides access to large amounts of historical and real-time data, making it possible to generate models and predictions of thermal related processes.

In this context, recent studies used the GEE platform to analyze the LST changes using MODIS and Landsat data. For example, de Almeida et al. [28] used annual summer and winter average LST MODIS and Landsat data acquired between 2003 and 2021 and analyzed the dynamics of the LST temporal trend in a mountainous area in Portugal. They figured out that the LST remained stable over time during summer but increased during winter nights. Bera et al. [29] used MODIS data to estimate the annual and seasonal day and night LST trends in relation to influencing factors from 2003 to 2020 in megacities of India using GEE. They found varying increases and decreases in LST between the different cities due to the variation in influencing factors in the day and night-time between the cities. Roy and Bari [30] examined the relationship between LST and LULC in Sylhet Sadar Upazila in southeastern Bangladesh using annual average of Landsat-5 and Landsat-8 LST images between 2000 and 2018. They found varying cooling and warming changes in LST due to the variation in LULC. Wang et al. [31] and Ermida et al. [27] created a GEE framework for producing global long time-series LST images using the entire Landsat thermal infrared image archive and evaluating it against in situ and MODIS LST products. Murtaza et al. [32] used GEE to evaluate the relationship between the spatiotemporal changes in urban areas and LST in Srinagar City in India using continuous archived time-

series Landsat imageries from 1992 to 2020 of summer months. The study revealed that the maximum and minimum LST average values has increased by 11 °C and 5 °C between 1992 and 2020, which indicated the impact of urbanization on the city.

In view of previous studies, assessing the LST trend over a longer period that fits climatological studies (i.e., +30 years) at local scales and monthly intervals would be essential for understanding the environmental changes. Here, analyzing the LST trend at LCZs in Jordan in the Middle East has been selected as the study area. Jordan has various LCZs enabling analyzing the influence of local natural variations on thermal behavior over time. The main objective of this study is to analyze the trend in LST over time using the entire archive of the available cloud-free Landsat images from 1986 to 2022 (36 years) for Jordan at monthly and LCZ scales. The study hypothesizes that the LST trend tends to increase at LCZs in Jordan due to climate change and other local characteristics (e.g., vegetation cover variation and LULC). This is the first study, to our knowledge, that analyzes the LST trend using continuous 36-year monthly Landsat time-series imageries over nine different LCZs at once. It would contribute to provide a better comprehensive understanding of LST impacts on Jordan’s LCZs for sustainable development and the demands on water resources management, food production, and energy supplies. GEE and Java scripts were used to perform the entire analyses.

3. Materials and Methods

3.1. Study Area

The entire geographic extent of Jordan in the Middle East was selected as the study area. It has nine various LCZs (Figure 1). In general, it is located within the Mediterranean climate zone, where the rainy season occurs from November to April while it is very dry for the rest of the year. The country covers an area of ~90,000 km² and located between 29° N and 34° N and 34° E and 40° E. Topographically, it is divided into three main landforms, namely the mountainous highlands, the desert plateau, and Jordan rift valley. Elevation extremes to the sea mean level are –408 m at the lowest point in the Dead Sea, and 1854 m at the highest point in Umm Dami mountain. The population is ~11.5 million inhabitants as of August 2023 (<http://dosweb.dos.gov.jo/>, accessed on 14 September 2023).

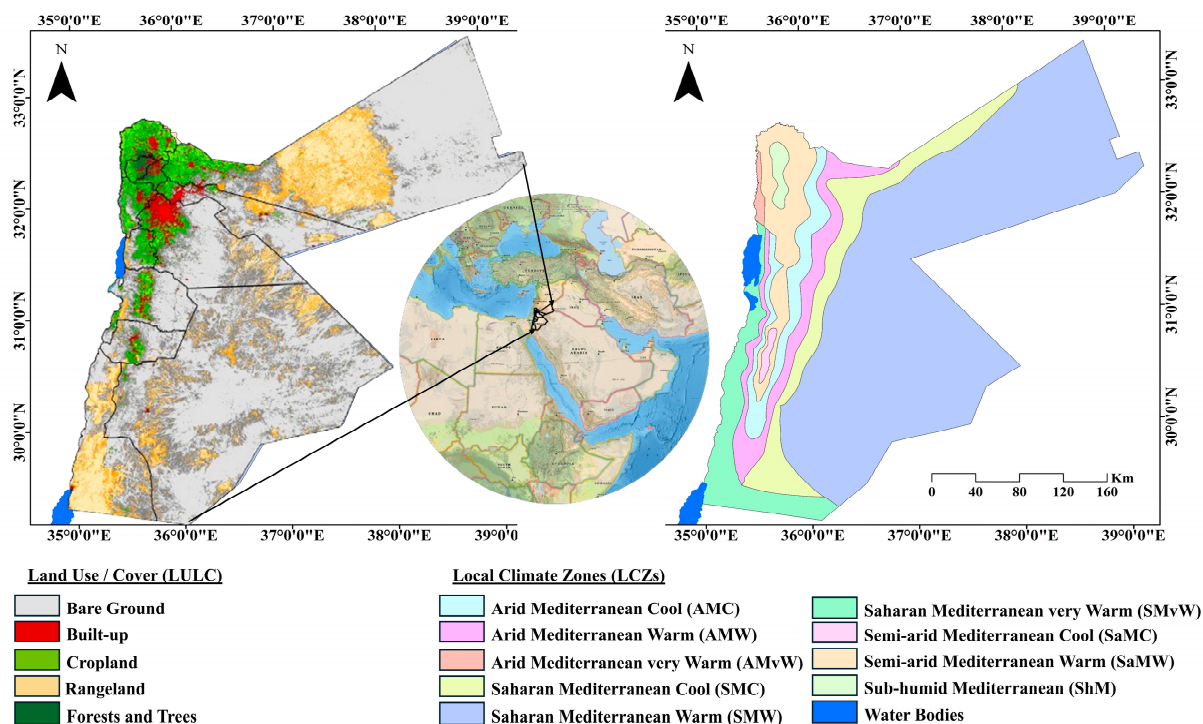


Figure 1. Map of Jordan (the study area) and its local climate zones (LCZs), after [33].

3.2. Data Used

Two primary datasets were used in this study: (i) Landsat-5; -8 imagery, and (ii) LCZs of Jordan. The entire archive of Landsat data at a spatial resolution of 30 m, between 1986 and 2022, was imported from the GEE catalog. The start and end dates were set between 1 January 1986 and 31 December 2022. The latest version (i.e., collection 2, level 2) of Landsat LST product was used because it has enhanced accuracy values over the previous versions. It was generated using the Landsat surface temperature algorithm (Version 1.3.0) that meets the <76 degrees' solar zenith angle constraint and includes the required auxiliary data inputs to generate a scientifically viable product [34]. Table 1 shows the parameters of Collection 2 LST enhancements.

Table 1. The parameters of Landsat Collection 2 LST enhancements *.

	Collection 2 Surface Temperature	Collection 1 Surface Temperature
Fill Value	0	−9999
Scaling Factor	$0.00341802 + 149.0$	0.1
Data Type	Unsigned 16-bit integer	Signed 16-bit integer
Valid Range	1–65,535	1500–3730
Atmospheric Reanalysis Source	GEOS-5 FP-IT (2000–present) MERRA-2 (1982–1999)	NARR
Quality Band	L1 QA_Pixel L1 QA_RADSAT L2 SR_QA_AEROSOL	Level-2 PIXELQA Level-2 RADSATQA Level-2 SRAEROSOLQA

* Source: USGS, <https://www.usgs.gov/landsat-missions/landsat-collection-2-level-2-science-products> (accessed on 16 August 2023).

The nine LCZs in Jordan were obtained from the Atlas of Jordan [34]. The Atlas was produced in 2013 and it contains key maps that support researchers in performing a spatial analysis of the environmental and socio-economical dynamics in Jordan. It was generated over seven years through collaboration between 48 Jordanian and international researchers from official and research departments [33].

3.3. Landsat Data Preparation

The archive of Landsat-5 Thematic Mapper (TM, band 6, 10.40–12.50 μm) and the Thermal Infrared Sensor (TIRS, band 10, 10.60–11.19 μm) of Landsat-8, in addition to the quality assessment masks (i.e., QA_PIXEL and QA_RADSAT) bands, were used to generate the monthly average LST images. All LST images were converted from digital numbers into Kelvin (K) units after applying a specific scale factor associated with the dataset (i.e., $\text{LST image} \times 0.00341802 + 149.0$). The QA bands were used to mask out any pixels that are contaminated by cloud and cloud shadow, or are saturated such as Bit 0—Fill, Bit 1—Dilated Cloud, Bit 2—Cirrus, Bit 3—Cloud, and Bit 4—Cloud Shadow. Finally, time-series of monthly LST images were prepared using compositing and mosaicking processes in which the compositing process was used to spatially combine the overlapping images into a single image based on an aggregation function (i.e., monthly mean), while the mosaicking process was used to assemble the spatially adjacent images into a spatially continuous images that cover the entire study area using the composited images. Then, all images were clipped within the boundary of Jordan using a boundary shapefile of the country. Note that the time-series of LST images for the period 1986–2010 were generated using Landsat-5 imageries, while the images between 2013 and 2022 were obtained from Landsat-8 imageries. The data for the period 2011–2012 were not available for the study area from these two data sources. Meanwhile, the data from Landsat-7 were not used due to its line-scan-error problem in the study area. These processes were performed using

cloud computing functions and Java scripts in GEE, enabling processing, and analyzing a total of 1,227,397 Landsat-5 and Landsat-8 images.

3.4. Estimating the LST Trends in Jordan and at Its LCZs Using Linear Regression Analysis

In GEE, the time-series images are represented in Image Collections, in which the data are joined together to define temporal relationships between the images using functions. The LST time-series is an array of the LST images sorted chronologically such as

$$pt = t0 + t1 \dots tN \quad (1)$$

where t is the LST image in the series. The first step in LST time-series analysis is to import the LST data and plot them within the area of interest. In this study, the area of interest was set to cover (i) the whole geographic extent of Jordan, and (ii) the nine LCZs. In both cases, the monthly averaged LST values were computed to evaluate the time-series trend. In both coverages, a strong seasonality and perhaps a gradual linear trend over time is hypothesized. Using Java script coding in the GEE platform, two functions called *addVariables* and *.map()* were created to extract the date and LST values of each image and store them in an array; and to build a time-series model of LST data, respectively. After that, a *.Chart()* function was used to visualize the linear trend line for LST over the period of interest (1986–2022). Ordinary Least Squares (OLS) was used to fit the trend model to the Landsat LST series by harnessing the *linearRegression()* reducer in GEE to estimate the linear trends over time. OLS tests were performed if the slope of the estimated linear regression line is different from zero.

3.5. Estimating the LST Trends in Jordan and at Its LCZs Using Mann-Kendall Test and Sen's Slope

The Mann–Kendall (MK) test and Sen's slope estimator (SSE) were used to detect the increasing or decreasing trends in LST and to quantify the magnitude of the trend, respectively in the study area over the period of interest. The variance of the MK test statistic, the Z-statistic for the test of presence of any trend, and the p -value of the statistic were also computed. The MK test is suitable for assessing monotonic trends over time, which measures whether the variable consistently increases/decreases over time, but the trend may or may not be linear [20]. It is measured as the sum of the signs of all the image pairs in the time-series. The SSE evaluates the magnitude and the direction of the trends such as warming or cooling in LST over time. It is the median slope of all image pairs in the time-series. The MK and SSE were calculated using the following equations:

$$MK = \sum_{k=1}^{n-1} \sum_{j=k+1}^n \text{sign}(x_j - x_k)$$

where

$$\text{sign}(x_j - x_k) = \begin{cases} +1 & \text{if } (x_j - x_k) > 0 \\ 0 & \text{if } (x_j - x_k) = 0 \\ -1 & \text{if } (x_j - x_k) < 0 \end{cases}$$

n is the number of image dates, and x_j and x_k are from $k = 1, 2, \dots, n - 1$ and $j = k + 1, \dots, n$ in the LST time-series. The mean of MK is 0, and the variance in MK is calculated as follows:

$$\text{var}(MK) = \frac{n(n-1)(2n+5)}{18}$$

when $n > 10$, the Z statistic is computed as follows:

$$Z = \begin{cases} \frac{MK-1}{\sqrt{var(MK)}} & \text{if } MK > 0 \\ 0 & \text{if } MK = 0 \\ \frac{MK+1}{\sqrt{var(MK)}} & \text{if } MK < 0 \end{cases}$$

Positive Z values indicate increasing trends while the negative Z values indicate decreasing trends.

The SSE is calculated as follows:

$$SSE = Median \left(\frac{x_j - x_i}{j - i} \right), j > i$$

where SEE is Sen’s slope for the set of pairs (i, x_i) in x_i time-series with the elements (x_i, x_j) fulfilling $j > i$. The negative SSE values indicate a cooling trend in the LST time-series, while the positive values indicate a warming trend. The data were tested at a 5% significance level. The null hypothesis (H_0) assumes that there is no trend in the series, while the alternative hypothesis (H_a) assumes that there is a trend in the series. If the computed p -value is lower than the significance level $\alpha = 0.05$, the null hypothesis (H_0) should be rejected, and the alternative hypothesis (H_a) is accepted.

4. Results and Discussion

4.1. Analysis of Minimum and Maximum LST Values during 1986–2022

Table 2 shows the long-term average minimum and maximum LST values for each climate zone in the country. It shows that the Semi-arid Mediterranean Cool zone witnessed the lowest minimum value at 284.0 K, while the Arid Mediterranean very Warm zone had the largest minimum value at 289.6 K. In terms of maximum LST values, the Saharan Mediterranean Warm zone had the largest maximum value at 323.2 K, while the Sub-humid Mediterranean zone witnessed the lowest maximum value at 315.8 K. The long-term standard deviation for the minimum LST values was greater than the that of the maximum LST values. This would indicate higher variation in minimum than maximum LST at all LCZs.

Table 2. The long-term average (LTA) minimum and maximum land surface temperature (LST) values and their standard deviations for each climate zone in Jordan.

Local Climate Zone	LTAmín	LTAmín_std	LTAmáx	LTAmáx_std
Saharan Mediterranean Warm (SMW)	287.6	3.2	323.2	2.9
Arid Mediterranean very Warm (AMvW)	289.6	4.3	320.4	2.4
Sub-humid Mediterranean (ShM)	285.8	3.2	315.8	2.4
Saharan Mediterranean very Warm (SMvW)	289.5	3.6	321.1	2.4
Saharan Mediterranean Cool (SMC)	286.5	3.8	321.2	2.6
Arid Mediterranean Cool (AMC)	285.2	3.9	318.3	2.2
Arid Mediterranean Warm (AMW)	286.2	3.9	318.9	2.4
Semi-arid Mediterranean Cool (SaMC)	284.0	5.0	316.8	2.5
Semi-arid Mediterranean Warm (SaMW)	285.1	4.0	318.3	2.4

Figure 2 shows the trend line for the annual minimum and maximum LST during the period 1986–2022. It shows a warming trend in the maximum LST values for all LCZs while there was annual fluctuation in the trend line of the minimum LST values in the zones. Though that both minimum and maximum LST vales would be affected over long periods, but often the maximum LST values would be more strongly influenced by long-term climate change due to different reasons such as (i) extreme heat events, which primarily affect maximum LST values, causing them to rise significantly during the hottest parts of the year—this effect is particularly pronounced in arid and semi-arid regions, which are prone to high temperature; (ii) increased evapotranspiration, which can lead to reduced soil moisture and plants water content. This can contribute to higher maximum LST values as the land surface heats up more quickly in drier conditions; (iii) changes in LULC can impact surface albedo, which affects the amount of solar radiation absorbed or reflected. Reduced vegetation cover and increased urban areas can lead to higher maximum LST values; and (iv) local geography such as elevation, proximity to water bodies, and topography can also influence the patterns of minimum LST values more than the maximum values.

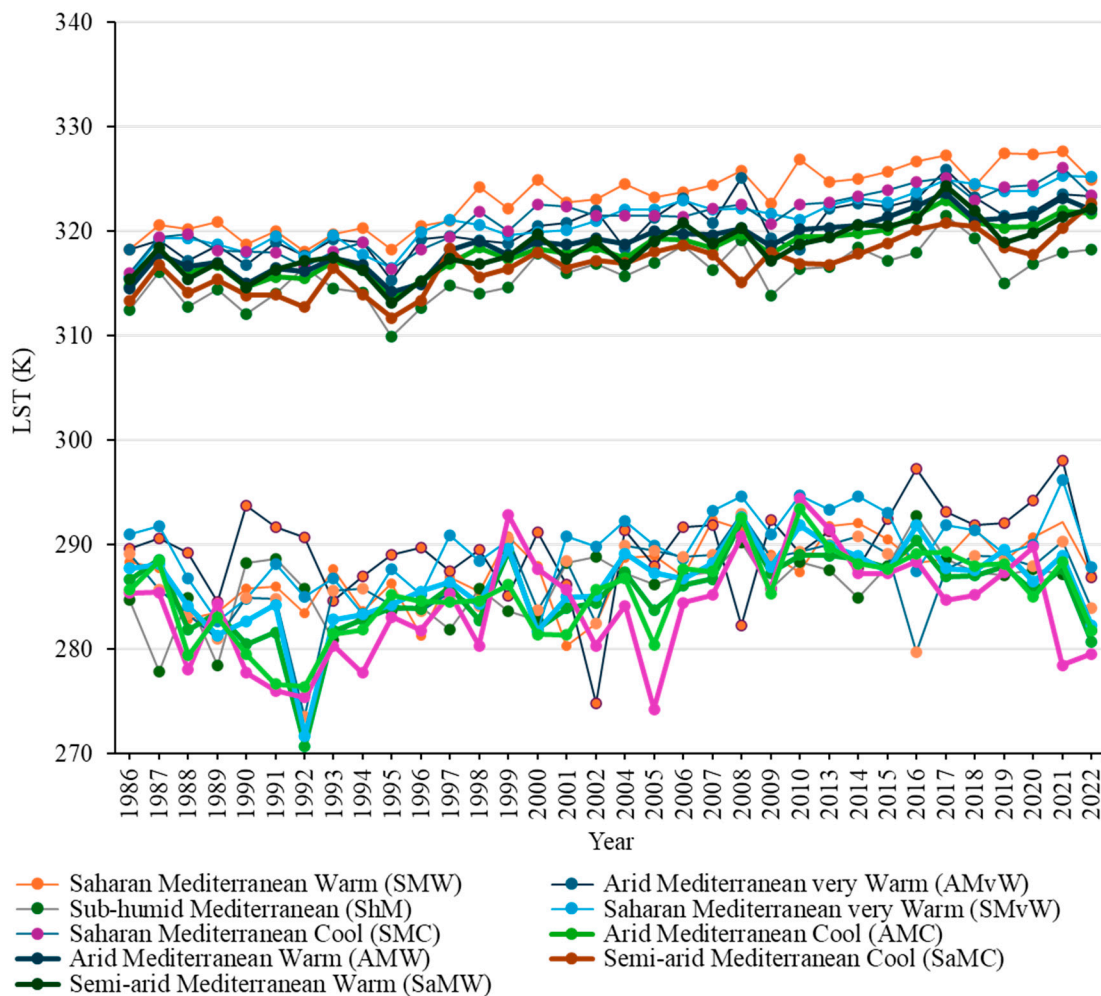


Figure 2. The trend line for the annual minimum and maximum land surface temperature (LST) during the period 1986–2022 for each local climate zone (LCZ).

4.2. LST Trend in Jordan and Its LCZs Using Linear Regression Analysis

Figure 3 shows the linear trend line of LST in Jordan during the period 1986–2022 using the entire available archive of Landsat-5 and Landsat-8 data. During this period, a noticeable trend in LST emerged. This trend is characterized by a persistent increase in LST across the country. The data show that the monthly average LST values have a

consistent upward trajectory, indicating a warming condition. This long-term trend in LST shows a substantial and persistent rise in temperatures. The magnitude of this increase is noteworthy, in fact, the average LST values have been progressively moving up year after year. For instance, the rate of change in LST (Slope = 0.0193 K/month) during this period highlights the importance of this trend surpassing the long-term average and suggesting a warming climate. While natural variations and annual fluctuations are expected in LST, the overall pattern at the country level transcends such short-term variability. This increase in monthly LST average values indicates a broader climate change phenomenon with possible far-reaching implications. Several factors could contribute to this warming trend, such as human activities and industrial processes, transportation, and deforestation, LULC change. Furthermore, studies have indicated that extreme climate events like heatwaves and prolonged high temperatures have become more frequent and severe in Jordan during this period, which further emphasized the impact of this LST trend [35,36]. These extreme events may have further consequences, affecting ecosystems, agriculture, water resources, and human health [36,37].

However, there would be regional variations in the intensity of this LST trend. Therefore, further analysis on LST trend was performed at LCZs in the country. Figure 4a–i shows that the trend in all climate zones was increasing, however, with variations in the rate of change (slope), which might be amplified or mitigated by local factors. For instance, the slope values ranged between 0.0117 K in the Sub-humid Mediterranean (ShM) zone (Figure 4c) to 0.0187 K in the Saharan Mediterranean Warm (SMW) zone (Figure 4a). This could be attributed to a combination of natural and anthropogenic factors. For example, (i) the proximity to Mediterranean Sea may have a moderating effect on LST as it acts as a heat reservoir, absorbing and releasing heat slowly, thereby stabilizing or mitigating warming trends in the ShM zone. In contrast, the SMW zone is located further inland, with less influence from the Mediterranean Sea. This leads to more extreme LST fluctuations, as there is less moderation from the sea. Meanwhile, the SMW zone is part of the Arabian Sahara Desert, which is known for its extreme heat and arid conditions. This can result in higher temperatures due to the strong influence of hot, dry air masses. (ii) Differences in elevation can also contribute to variations in LST. The ShM zone has higher elevation as it represents the mountains in the country, which have cooler temperatures compared to low-lying areas in the SMW zone. (iii) Differences in land use and agricultural practices between the zones can also affect local LST. The ShM zone contains most of the agricultural land and forested areas [34], which can reduce the warming trend by adding moisture to the air, while the vegetation cover in the SMW zone is rare. It is important to note that these factors can interact in complex ways, and the rate of LST change could be influenced by all of them.

Table 3 shows summary of the annual rate of change (slope) of LST for each climate zone; it shows that the three Saharan zones are experiencing the highest rate of LST increase at 0.0184 K/year for SMW, 0.0184 K/year for SMC, and 0.0196 K/year for SMvW, indicating rapid warming in these regions. The three arid zones come in the middle with values of 0.0156 K/year for AMW, 0.0151 for AMvW, and 0.0139 for AMC, suggesting a slower warming trend. The two semi-arid zones and the sub-humid zone show lower values at 0.0138, 0.0127, and 0.0117 K/year for SaMC, SaMW, and ShM zones, respectively, suggesting the lowest rate of change compared to other zones.

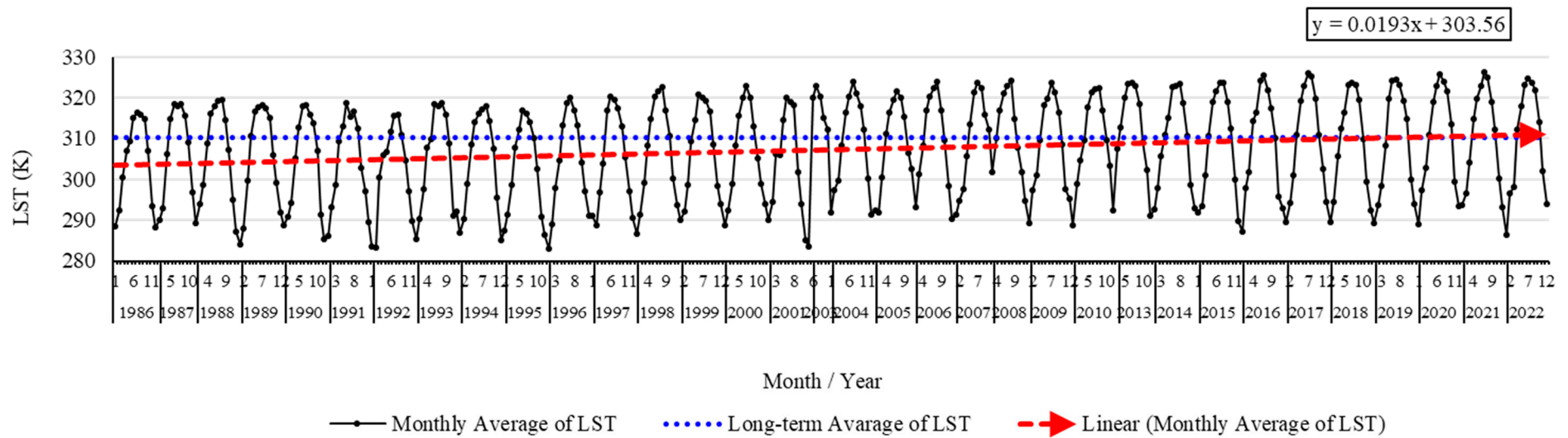


Figure 3. Trend analysis of LST over Jordan between 1986 and 2022.

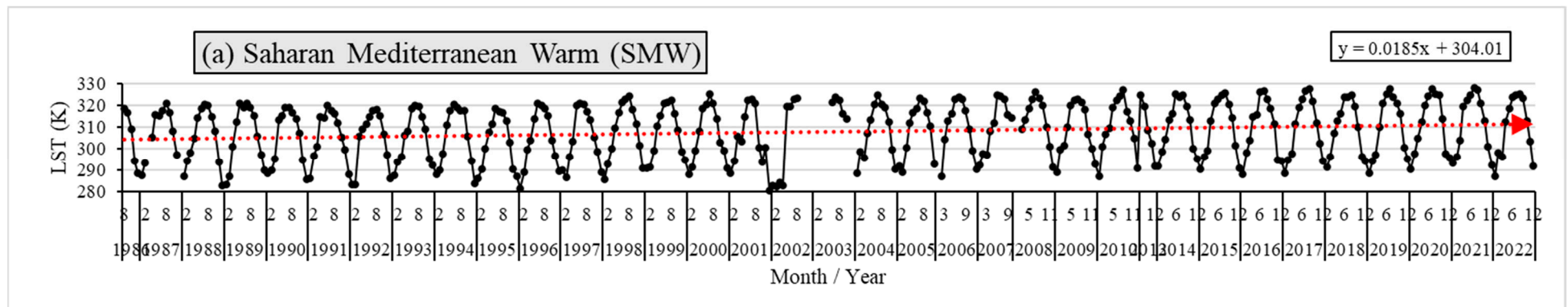


Figure 4. Cont.

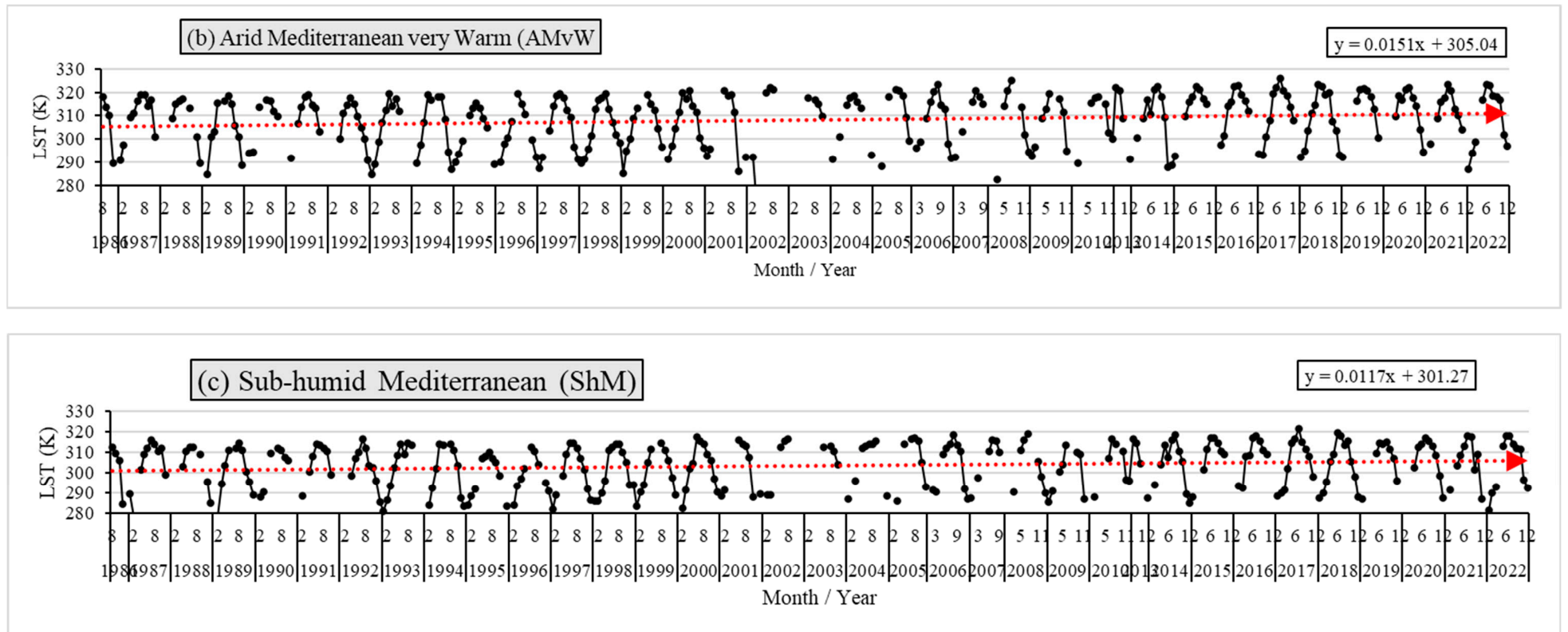


Figure 4. Cont.

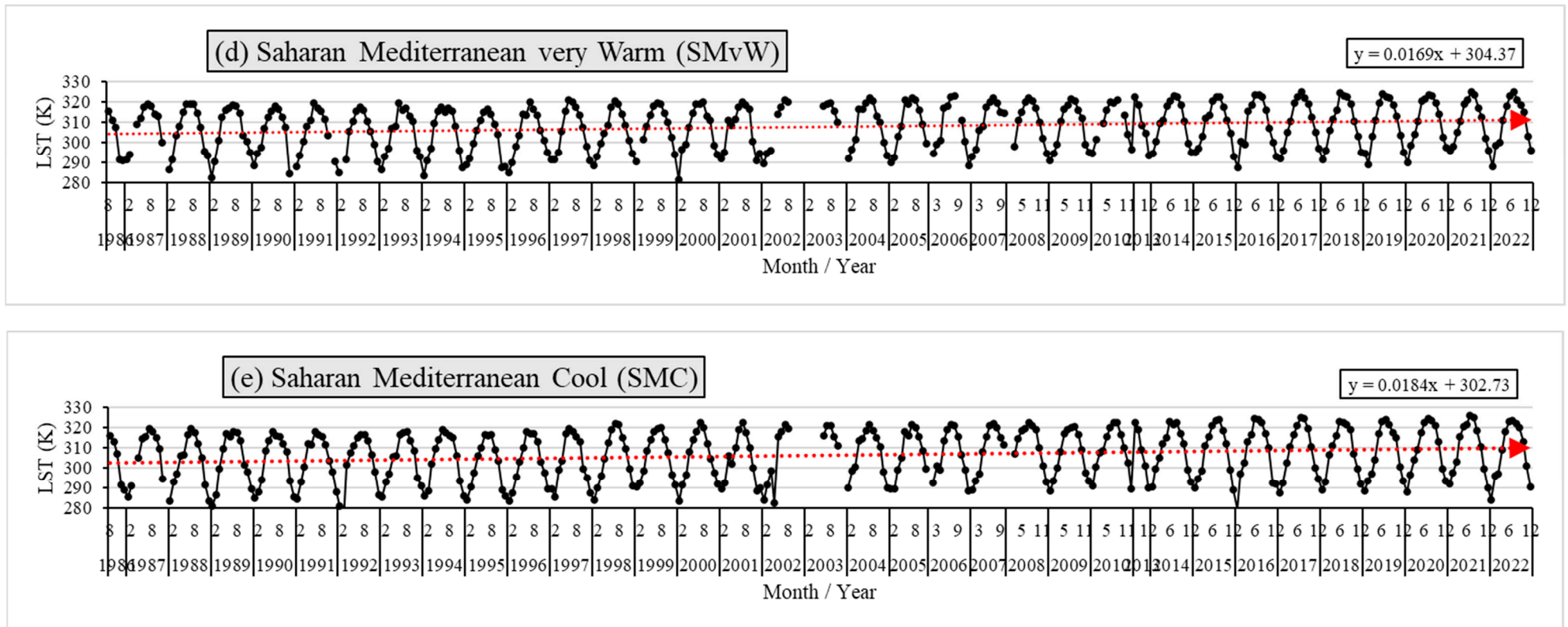


Figure 4. Cont.

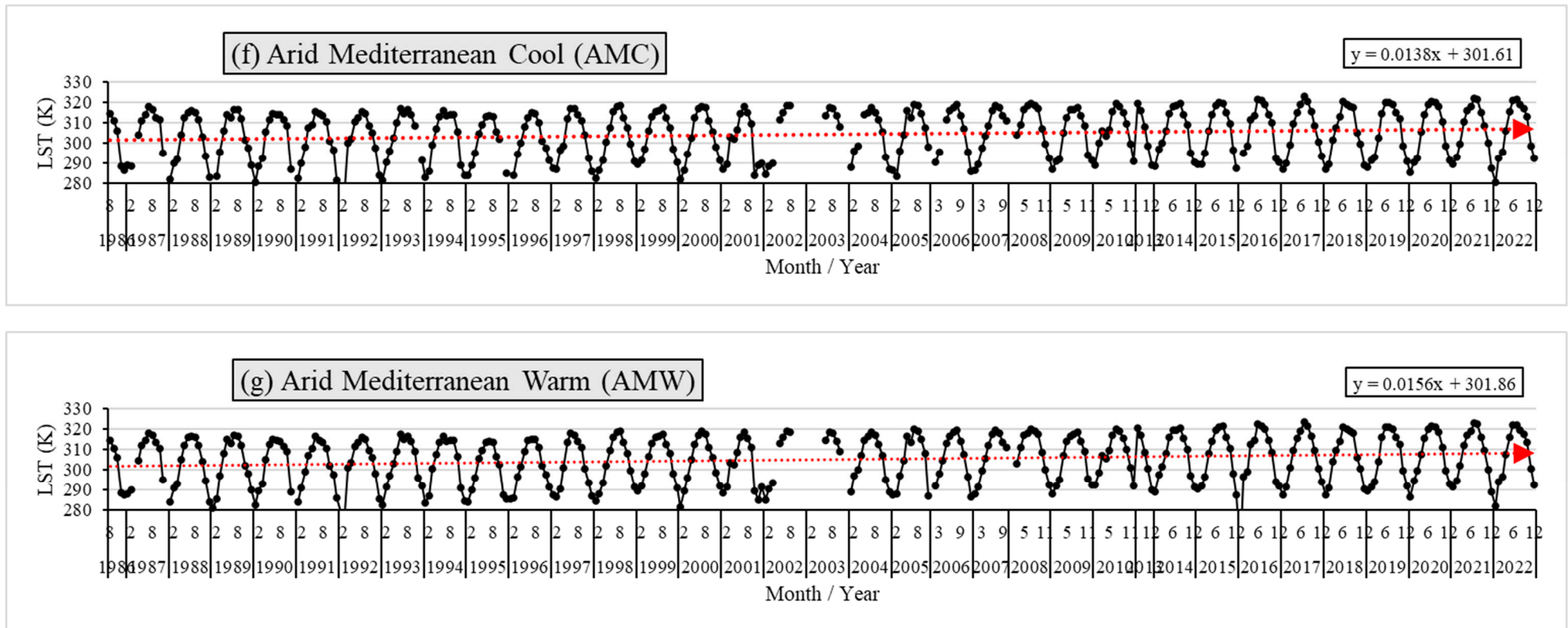


Figure 4. Cont.

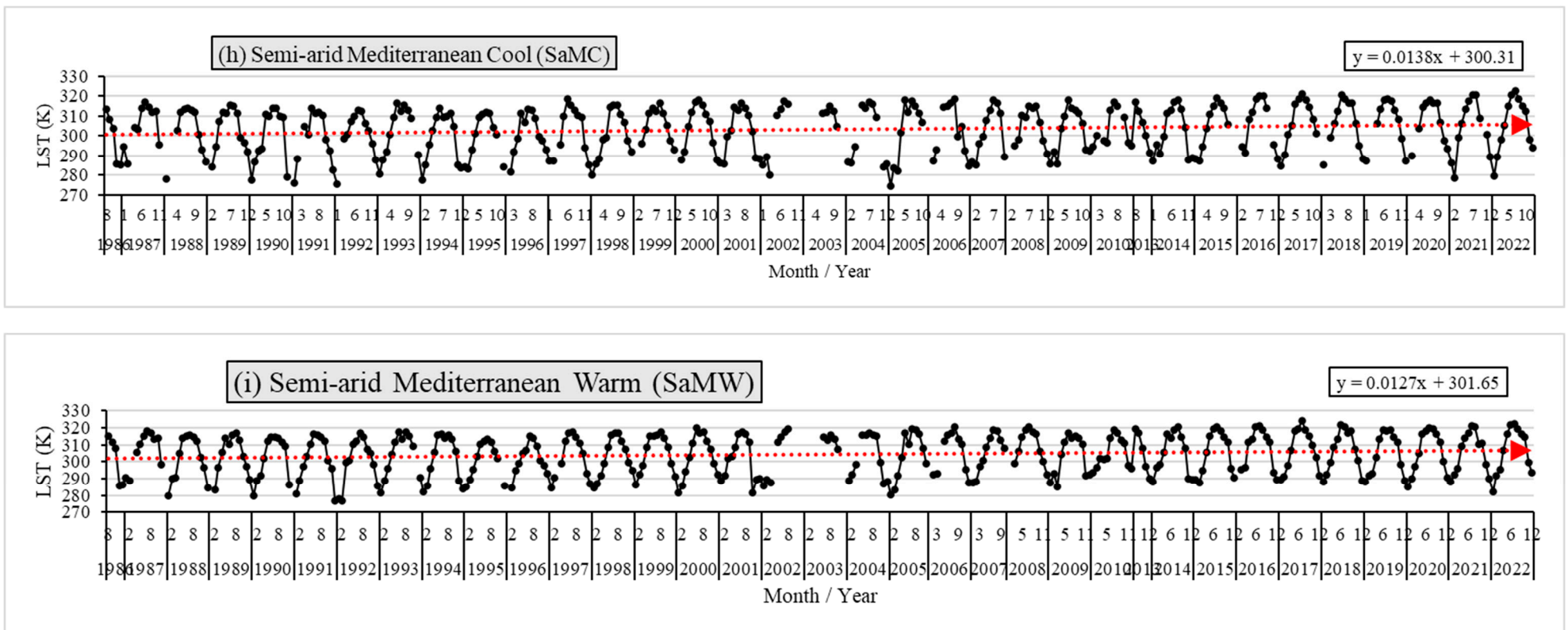


Figure 4. Trend analysis of LST over local climate zones (LCZs) in Jordan between 1986 and 2022. The red arrows represents the trend line of the monthly long-term average of land surface temperature (LST).

Table 3. Annual rate of change (slope) of LST for each climate zone in Jordan in an ascending order.

Local Climate Zone	Rate of Change (Slope) K/Year
Sub-humid Mediterranean (ShM)	0.0117
Semi-arid Mediterranean Warm (SaMW)	0.0127
Semi-arid Mediterranean Cool (SaMC)	0.0138
Arid Mediterranean Cool (AMC)	0.0139
Arid Mediterranean very Warm (AMvW)	0.0151
Arid Mediterranean Warm (AMW)	0.0156
Saharan Mediterranean very Warm (SMvW)	0.0169
Saharan Mediterranean Cool (SMC)	0.0184
Saharan Mediterranean Warm (SMW)	0.0185

4.3. LST Trend at LCZs in Jordan Using the Mann–Kendall Trend Test and Sen’s Slope Estimator

Figure 5 and Table 4 show the trends of LST in the LCZs in Jordan as calculated using MK and SSE. The results showed an existing warming trend in both monthly and annual levels in all LCZs in Jordan during the period 1986–2022 at statistically significant levels with 95% confidence. The average maximum warming trend value was 0.204 K/year at the monthly scale. The Saharan Mediterranean Warm (SMW) climate zone scored the highest warming trends in six months (i.e., April, June, July, August, September, and December) and at the annual level. This is the driest zone in the country and the vegetation cover is missing except for a few farms that depend on pumping underground water; such environment may truly witness the highest impact of the local warming trend. The average minimum trend value was 0.105 K/year on the monthly scale. The Sub-humid Mediterranean (ShM) scored the minimum warming trends at the annual level and all months except in February and October. This might refer to the topography and vegetation cover in this zone as it is in the mountainous area in the country and contains the ever-green forested area in Jordan; these factors may reduce or flatten the change in the warming trend. Figure 6 shows the temporal variation in LST in the LCZs in Jordan. It shows that the Sub-humid Mediterranean zone witnessed the maximum variation, with slope values ranging between 0.017 K/year in March and 0.244 K/year in February. The Arid Mediterranean Warm zone had the lowest variation, with slope values between 0.122 K/year in December and 0.194 K/year in August.

Table 4. Slope values (rate of change) of monthly average and annual land surface temperature (LST) for each local climate zone (LCZ) in Jordan as calculated by Sen’s slope estimator.

LCZs	Jan	Feb	Mar	Apr	May	Jun	Jul	Aug	Sep	Oct	Nov	Dec	Annual
SMW	0.127	0.218	<i>0.101</i>	0.171	0.171	0.193	0.262	0.237	0.217	0.197	0.173	0.215	0.190
AMvW	<i>0.098</i>	0.159	<i>0.105</i>	0.119	0.124	0.124	0.189	0.124	0.178	0.176	<i>0.099</i>	0.176	0.139
ShM	<i>0.067</i>	0.244	<i>0.017</i>	<i>0.080</i>	<i>0.055</i>	<i>0.102</i>	0.168	0.100	0.080	0.185	<i>0.038</i>	<i>0.097</i>	0.103
SMvW	0.201	0.183	0.176	0.125	0.207	0.180	0.202	0.210	0.195	0.193	0.214	0.119	0.184
SMC	0.153	0.231	0.155	0.119	0.188	0.193	0.221	0.223	0.213	0.189	0.182	0.159	0.186
AMC	0.177	0.159	<i>0.096</i>	0.116	0.115	0.175	0.190	0.161	0.156	0.177	0.139	0.141	0.150
AMW	0.175	0.181	0.134	0.131	0.132	0.182	0.197	0.194	0.189	0.164	0.154	0.122	0.163
SaMC	<i>0.203</i>	<i>0.146</i>	<i>0.103</i>	<i>0.102</i>	0.142	0.169	0.211	0.154	0.131	0.137	0.164	0.130	0.149
SaMW	0.208	0.173	0.059	0.099	0.107	0.154	0.194	0.132	0.129	0.204	<i>0.107</i>	<i>0.136</i>	0.142
Average	0.156	0.188	0.105	0.118	0.138	0.164	0.204	0.171	0.165	0.180	0.141	0.144	0.156

Note: The slope values in italics are for trends that were not significant (i.e., the computed *p*-value was lower than the significance level alpha = 0.05).

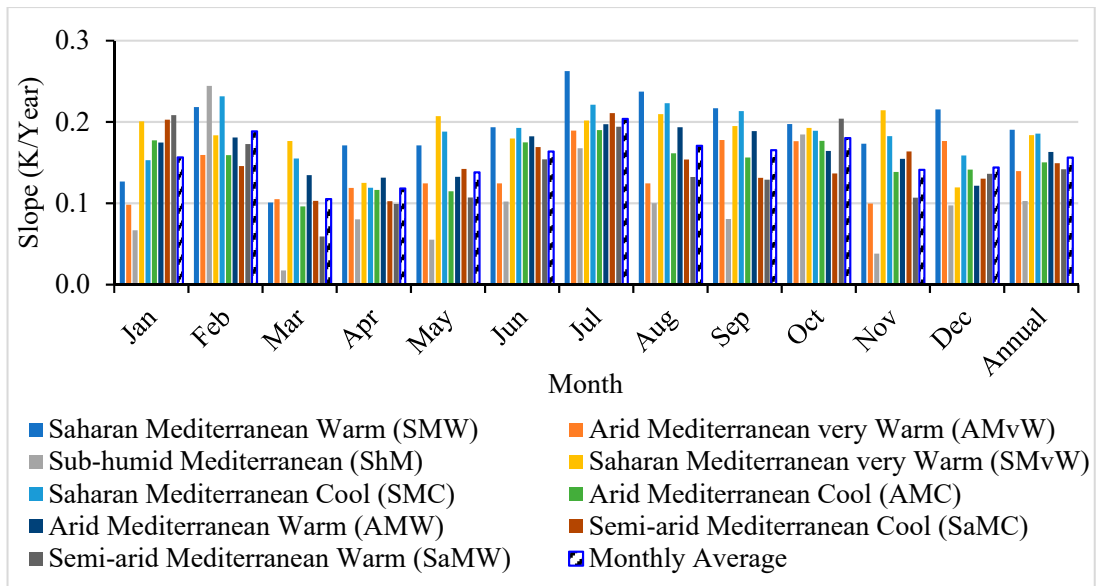


Figure 5. LST warming trends in the local climate zones (LCZs) in Jordan. The confidence level of the Mann–Kendall (MK) test and Sen’s slope estimator (SSE) is 95%.

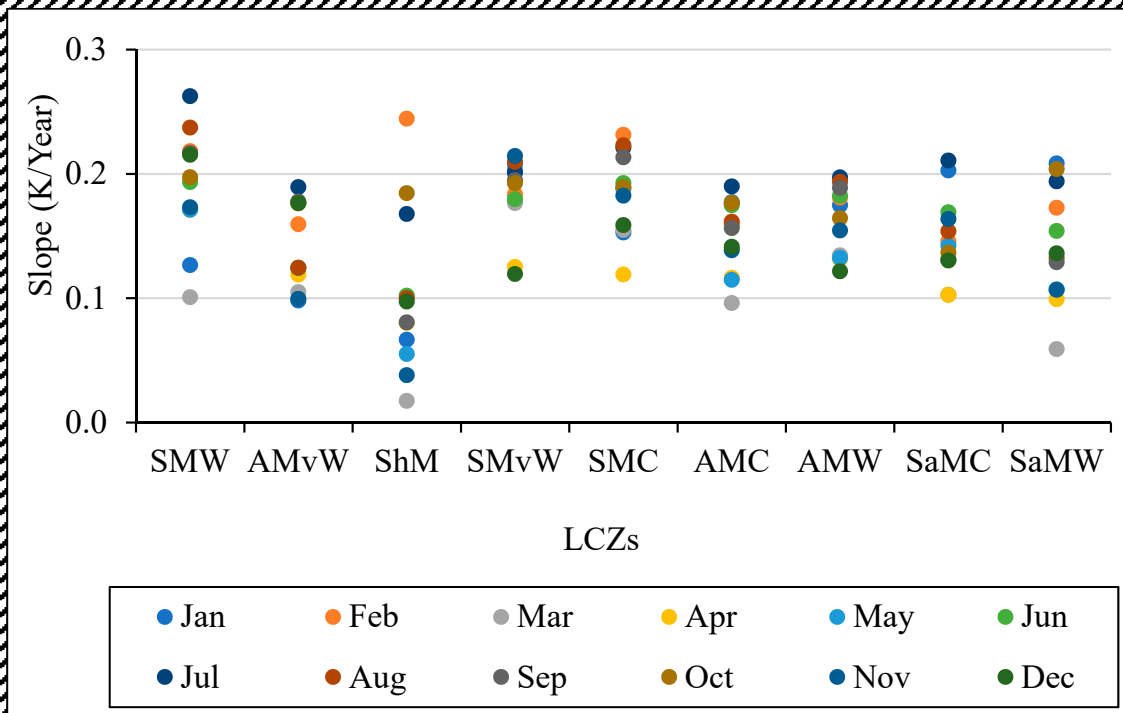


Figure 6. Temporal variation in land surface temperature in local climate zones in Jordan. Sub-humid Mediterranean (ShM), Semi-arid Mediterranean Warm (SaMW), Semi-arid Mediterranean Cool (SaMC), Arid Mediterranean Cool (AMC), Arid Mediterranean very Warm (AMvW), Arid Mediterranean Warm (AMW), Saharan Mediterranean very Warm (SMvW), Saharan Mediterranean Cool (SMC), and Saharan Mediterranean Warm (SMW) zones.

5. Discussion

The analysis of the LST trend in Jordan across various climate zones and timeframes offered valuable insights into regional variations and drivers of change. The observed pattern of the long-term LST aligns with established global trends of rising LSTs, mirroring findings in studies like in [14,17]. The lowest minimum LST in the Semi-arid Mediterranean

Cool zone and the highest in the Arid Mediterranean Very Warm zone are consistent with expected climatic differences; such differences in LST values between these two zones reflect their distinct climatic characteristics, with the Semi-arid Mediterranean Cool zone being relatively cooler due to moderating influences, while the Arid Mediterranean Very Warm zone exhibits higher temperatures typical of arid environments; this coincides with findings in [38,39]. Interestingly, the higher standard deviation for minimum LSTs compared to maximums suggests greater fluctuations in minimum temperatures across all zones. This could be attributed to complex interactions between local factors like topography and prevailing winds. The consistent warming trend in maximum LSTs across all zones confirms the impact of climate change on Jordan, echoing global observations [14,17].

However, the results highlight significant regional variations in the rate of warming. The three Saharan zones experiencing the highest LST increase are likely due to their arid conditions and lack of moderating factors like water bodies. Conversely, the Sub-humid Mediterranean zone with its higher elevation and vegetation cover exhibits the lowest warming rate, supporting observations by [23] on the mitigating effects of these factors. The other factors contributing to the influence of climate change on maximum LSTs such as extreme heat events align with findings by Zeitoun and Jaradat [38] and are particularly pronounced in arid regions [35,36]. The increased evapotranspiration dries the land surface, leading to faster heating, as seen in other studies [3]. Meanwhile, LULC change reduces vegetation cover and can significantly raise maximum LSTs, as demonstrated in [23].

The identified regional variations and driving factors highlight the need for further research at finer spatial scales to understand the specific mechanisms governing LST changes in different zones. Investigating the interplay between local factors (e.g., topography, water bodies) and broader climate trends could provide valuable insights for targeted adaptation strategies. Meanwhile, exploring the potential impacts of LST changes on various environmental and socio-economic aspects in Jordan could inform policy and resource management decisions. This would provide a comprehensive understanding of LST patterns and their drivers for developing effective adaptation strategies to mitigate the impacts of climate change on the country's ecosystems and communities.

6. Conclusions

This study analyzed the trend of LST between 1986 and 2022 in Jordan and its nine LCZs using the entire archive of available Landsat data within the study area. Different statistical analyses were performed to understand the LST trend. The results showed that LST is on an upward trajectory in the study area, with potentially profound consequences for its climate and environmental regimes. This trend was observed at the scale of the country and at the local climate zones. The spatiotemporal variations in LST in the study area and its associated driving factors were demonstrated. LULC types, natural vegetation, elevation variation, and proximity to open water bodies are the main influential factors. Addressing this warming trend and mitigating its effects are critical challenges that require attention and concerted efforts to reduce the warming driven by human-induced factors and worsened by extreme events and LULC change and adapting to the changing climate. Understanding and addressing this trend is vital for preservation of the environment, ecosystems, and human well-being in the face of a changing climate within the local climate zones in Jordan and improving the sustainable development plans.

Author Contributions: Conceptualization, K.H. and A.A.; methodology, K.H.; validation, A.A.R. and M.Z.; formal analysis, K.H.; writing—original draft preparation, K.H.; writing—review and editing, A.A., M.Z. and A.A.R. All authors have read and agreed to the published version of the manuscript.

Funding: This research received no external funding.

Institutional Review Board Statement: Not applicable.

Informed Consent Statement: Not applicable.

Data Availability Statement: The data presented in this study are available on request from the corresponding author. The data are not publicly available as they were generated through specific codes in Google Earth Engine (GEE) by the corresponding author.

Acknowledgments: The authors would like to thank the United States Geological Survey (USGS) for providing the Landsat. Many thanks to Google for providing the Google Earth Engine platform for public use.

Conflicts of Interest: The authors declare no conflicts of interest. The roles in the collection, analyses, or interpretation of data; in the writing of the manuscript, and the decision to publish the results are solely by the authors.

References

1. Yang, J.; Ren, J.; Sun, D.; Xiao, X.; Xia, J.C.; Jin, C.; Li, X. Understanding Land Surface Temperature Impact Factors Based on Local Climate Zones. *Sustain. Cities Soc.* **2021**, *69*, 102818. [\[CrossRef\]](#)
2. Stewart, I.D.; Oke, T.R.; Krayenhoff, E.S. Evaluation of the ‘Local Climate Zone’ Scheme Using Temperature Observations and Model Simulations. *Int. J. Climatol.* **2014**, *34*, 1062–1080. [\[CrossRef\]](#)
3. Allan, R.P.; Barlow, M.; Byrne, M.P.; Cherchi, A.; Douville, H.; Fowler, H.J.; Gan, T.Y.; Pendergrass, A.G.; Rosenfeld, D.; Swann, A.L. Advances in Understanding Large-Scale Responses of the Water Cycle to Climate Change. *Ann. N. Y. Acad. Sci.* **2020**, *1472*, 49–75. [\[CrossRef\]](#) [\[PubMed\]](#)
4. Sillero, N. Climate Change in Action: Local Elevational Shifts on Iberian Amphibians and Reptiles. *Reg. Environ. Chang.* **2021**, *21*, 101. [\[CrossRef\]](#)
5. Fricke, C.; Pongrácz, R.; Gál, T.M.; Savić, S.; Unger, J. Using Local Climate Zones to Compare Remotely Sensed Surface Temperatures in Temperate Cities and Hot Desert Cities. *Morav. Geogr. Rep.* **2020**, *28*, 48–60. [\[CrossRef\]](#)
6. Geletič, J.; Lehnert, M.; Dobrovolný, P. Land Surface Temperature Differences within Local Climate Zones, Based on Two Central European Cities. *Remote Sens.* **2016**, *8*, 788. [\[CrossRef\]](#)
7. Yang, X.; Yao, L.; Jin, T.; Peng, L.L.; Jiang, Z.; Hu, Z.; Ye, Y. Assessing the Thermal Behavior of Different Local Climate Zones in the Nanjing Metropolis, China. *Build. Environ.* **2018**, *137*, 171–184. [\[CrossRef\]](#)
8. Wulder, M.A.; Roy, D.P.; Radeloff, V.C.; Loveland, T.R.; Anderson, M.C.; Johnson, D.M.; Healey, S.; Zhu, Z.; Scambos, T.A.; Pahlevan, N. Fifty Years of Landsat Science and Impacts. *Remote Sens. Environ.* **2022**, *280*, 113195. [\[CrossRef\]](#)
9. Sattari, F.; Hashim, M. A Brief Review of Land Surface Temperature Retrieval Methods from Thermal Satellite Sensors. *Middle-East J. Sci. Res.* **2014**, *22*, 757–768.
10. Li, Z.-L.; Wu, H.; Duan, S.-B.; Zhao, W.; Ren, H.; Liu, X.; Leng, P.; Tang, R.; Ye, X.; Zhu, J. Satellite RS of Global Land Surface Temperature: Definition, Methods, Products, and Applications. *Rev. Geophys.* **2023**, *61*, e2022RG000777. [\[CrossRef\]](#)
11. Nega, W.; Balew, A. The Relationship between Land Use Land Cover and Land Surface Temperature Using RS: Systematic Reviews of Studies Globally over the Past 5 Years. *Environ. Sci. Pollut. Res.* **2022**, *29*, 42493–42508. [\[CrossRef\]](#) [\[PubMed\]](#)
12. Jaber, S.M.; Abu-Allaban, M.M. MODIS-Based Land Surface Temperature for Climate Variability and Change Research: The Tale of a Typical Semi-Arid to Arid Environment. *Eur. J. Remote Sens.* **2020**, *53*, 81–90. [\[CrossRef\]](#)
13. Luintel, N.; Ma, W.; Ma, Y.; Wang, B.; Subba, S. Spatial and Temporal Variation of Daytime and Nighttime MODIS Land Surface Temperature across Nepal. *Atmos. Ocean. Sci. Lett.* **2019**, *12*, 305–312. [\[CrossRef\]](#)
14. Dewan, A.; Kiselev, G.; Botje, D.; Mahmud, G.I.; Bhuian, M.H.; Hassan, Q.K. Surface Urban Heat Island Intensity in Five Major Cities of Bangladesh: Patterns, Drivers and Trends. *Sustain. Cities Soc.* **2021**, *71*, 102926. [\[CrossRef\]](#)
15. Eleftheriou, D.; Kiachidis, K.; Kalmintzis, G.; Kalea, A.; Bantasis, C.; Koumadoraki, P.; Spathara, M.E.; Tsolaki, A.; Tzampazidou, M.I.; Gemitzi, A. Determination of Annual and Seasonal Daytime and Nighttime Trends of MODIS LST over Greece—Climate Change Implications. *Sci. Total Environ.* **2018**, *616*, 937–947. [\[CrossRef\]](#) [\[PubMed\]](#)
16. Hassan, Q.K.; Ejiagha, I.R.; Ahmed, M.R.; Gupta, A.; Rangelova, E.; Dewan, A. RS of Local Warming Trend in Alberta, Canada during 2001–2020, and Its Relationship with Large-Scale Atmospheric Circulations. *Remote Sens.* **2021**, *13*, 3441. [\[CrossRef\]](#)
17. Yang, M.; Zhao, W.; Zhan, Q.; Xiong, D. Spatiotemporal Patterns of Land Surface Temperature Change in the Tibetan Plateau Based on MODIS/Terra Daily Product from 2000 to 2018. *IEEE J. Sel. Top. Appl. Earth Obs. Remote Sens.* **2021**, *14*, 6501–6514. [\[CrossRef\]](#)
18. Liu, J.; Hagan, D.F.T.; Liu, Y. Global Land Surface Temperature Change (2003–2017) and Its Relationship with Climate Drivers: AIRS, MODIS, and ERA5-Land Based Analysis. *Remote Sens.* **2020**, *13*, 44. [\[CrossRef\]](#)
19. Yan, Y.; Mao, K.; Shi, J.; Piao, S.; Shen, X.; Dozier, J.; Liu, Y.; Ren, H.; Bao, Q. Driving Forces of Land Surface Temperature Anomalous Changes in North America in 2002–2018. *Sci. Rep.* **2020**, *10*, 6931. [\[CrossRef\]](#)
20. Shawky, M.; Ahmed, M.R.; Ghaderpour, E.; Gupta, A.; Achari, G.; Dewan, A.; Hassan, Q.K. RS-Derived Land Surface Temperature Trends over South Asia. *Ecol. Inform.* **2023**, *74*, 101969. [\[CrossRef\]](#)
21. Fu, P.; Weng, Q. Temporal Dynamics of Land Surface Temperature from Landsat TIR Time Series Images. *IEEE Geosci. Remote Sens. Lett.* **2015**, *12*, 2175–2179.

22. Sekertekin, A.; Arslan, N.; Bilgili, M. Modeling Diurnal Land Surface Temperature on a Local Scale of an Arid Environment Using Artificial Neural Network (ANN) and Time Series of Landsat-8 Derived Spectral Indexes. *J. Atmos. Sol.-Terr. Phys.* **2020**, *206*, 105328. [CrossRef]
23. Athick, A.M.A.; Shankar, K.; Naqvi, H.R. Data on Time Series Analysis of Land Surface Temperature Variation in Response to Vegetation Indices in Twelve Wereda of Ethiopia Using Mono Window, Split Window Algorithm and Spectral Radiance Model. *Data Brief* **2019**, *27*, 104773. [CrossRef] [PubMed]
24. Gorelick, N.; Hancher, M.; Dixon, M.; Ilyushchenko, S.; Thau, D.; Moore, R. Google Earth Engine: Planetary-Scale Geospatial Analysis for Everyone. *Remote Sens. Environ.* **2017**, *202*, 18–27. [CrossRef]
25. Amani, M.; Ghorbanian, A.; Ahmadi, S.A.; Kakooei, M.; Moghimi, A.; Mirmazloumi, S.M.; Moghaddam, S.H.A.; Mahdavi, S.; Ghahremanloo, M.; Parsian, S. Google Earth Engine Cloud Computing Platform for RS Big Data Applications: A Comprehensive Review. *IEEE J. Sel. Top. Appl. Earth Obs. Remote Sens.* **2020**, *13*, 5326–5350. [CrossRef]
26. Tamiminia, H.; Salehi, B.; Mahdianpari, M.; Quackenbush, L.; Adeli, S.; Brisco, B. Google Earth Engine for Geo-Big Data Applications: A Meta-Analysis and Systematic Review. *ISPRS J. Photogramm. Remote Sens.* **2020**, *164*, 152–170. [CrossRef]
27. Ermida, S.L.; Soares, P.; Mantas, V.; Göttsche, F.-M.; Trigo, I.F. Google Earth Engine Open-Source Code for Land Surface Temperature Estimation from the Landsat Series. *Remote Sens.* **2020**, *12*, 1471. [CrossRef]
28. de Almeida, C.R.; Garcia, N.; Campos, J.C.; Alirio, J.; Arenas-Castro, S.; Gonçalves, A.; Sillero, N.; Teodoro, A.C. Time-Series Analyses of Land Surface Temperature Changes with Google Earth Engine in a Mountainous Region. *Heliyon* **2023**, *9*, e18846. [CrossRef]
29. Bera, D.; Chatterjee, N.D.; Ghosh, S.; Dinda, S.; Bera, S. Recent Trends of Land Surface Temperature in Relation to the Influencing Factors Using Google Earth Engine Platform and Time Series Products in Megacities of India. *J. Clean. Prod.* **2022**, *379*, 134735. [CrossRef]
30. Roy, B.; Bari, E. Examining the Relationship between Land Surface Temperature and Landscape Features Using Spectral Indices with Google Earth Engine. *Heliyon* **2022**, *8*, e10668. [CrossRef] [PubMed]
31. Wang, M.; Zhang, Z.; Hu, T.; Wang, G.; He, G.; Zhang, Z.; Li, H.; Wu, Z.; Liu, X. An Efficient Framework for Producing Landsat-Based Land Surface Temperature Data Using Google Earth Engine. *IEEE J. Sel. Top. Appl. Earth Obs. Remote Sens.* **2020**, *13*, 4689–4701. [CrossRef]
32. Murtaza, K.O.; Shafai, S.; Shahid, P.; Romshoo, S.A. Understanding the Linkages between Spatio-Temporal Urban Land System Changes and Land Surface Temperature in Srinagar City, India, Using Image Archives from Google Earth Engine. *Environ. Sci. Pollut. Res. Int.* **2023**, *30*, 107281–107295. [CrossRef]
33. Ababsa, M. (Ed.) *Atlas of Jordan: History, Territories and Society*; Contemporain publications; Presses de l’Ifpo: Beyrouth, Lebanon, 2014; ISBN 978-2-35159-438-4.
34. Cook, M.; Schott, J.R.; Mandel, J.; Raqueno, N. Development of an Operational Calibration Methodology for the Landsat Thermal Data Archive and Initial Testing of the Atmospheric Compensation Component of a Land Surface Temperature (LST) Product from the Archive. *Remote Sens.* **2014**, *6*, 11244–11266. [CrossRef]
35. Alwadi, Y.; Abdulla, F. Spatiotemporal Analysis of Heat Waves in Jordan. Available online: <https://www.researchsquare.com> (accessed on 16 September 2023).
36. Al-Hadidi, L.; Sweity, A. Potential Impact of Climate Change on Shifting the Calendar of Rainfed Crops Produced in Jordan. *Int. J. Glob. Warm.* **2023**, *30*, 282–295. [CrossRef]
37. Shehadeh, N.; Tarawneh, F. Impact of Climate Change upon Summer heat Waves in Jordan. *J. Am. Sci.* **2014**, *10*, 46–52.
38. Zeitoun, M.; Jaradat, S. Estimation of the Earth surface temperature using LANDSAT 8 sensor data: In Irbid during the heat waves 2020: A case study. *Assoc. Arab. Univ. J. Arts* **2024**, *21*, 21–51.
39. Zeitoun, M. Analysis of Temperature Anomalies During the Spring Months in Jordan. *Int. J. Geoinformatics* **2024**, *20*, 88–98. [CrossRef]

Disclaimer/Publisher’s Note: The statements, opinions and data contained in all publications are solely those of the individual author(s) and contributor(s) and not of MDPI and/or the editor(s). MDPI and/or the editor(s) disclaim responsibility for any injury to people or property resulting from any ideas, methods, instructions or products referred to in the content.